

Inducing Extraordinarily Piezoelectric Response via Homogeneous and Heterogeneous Functionalization of a Sc_2C Nanosheet, A Quantum Chemical Investigation

Khaled E. El-Kelany,¹ Safwat Abdel-Azeim,² Oliver Kühn,³ Ahmed El-Zatahry,⁴ and Mohamed F. Shibl⁵

¹*Institute of Nanoscience and Nanotechnology, Kafrelshiekh University, 33516 Kafrelshiekh, Egypt*

²*Center for Integrative Petroleum Research (CIPR),
College of Petroleum Engineering and Geosciences,*

King Fahd University of Petroleum and Minerals (KFUPM), Dhahran 31261, Saudi Arabia

³*Institut für Physik, Universität Rostock, Albert-Einstein-Str. 23-24, D-18059 Rostock, Germany*

⁴*Material Science and Technology Program, College of Arts and Sciences, Qatar University, 2713, Doha, Qatar*

⁵*Renewable Energy Program, Center for Sustainable Development,
College of Arts and Sciences, Qatar University, 2713 Doha, Qatar**

(Dated: January 26, 2023)

Piezoelectricity is pivotal for applications in micro/nanoelectromechanical (MEMS/NEMS) systems. Inducing such property into the two-dimensional $\text{Sc}_2\text{CTT}'$ MXenes (where T and T' are the functionalization atoms) via homogeneous and heterogeneous surface functionalization is explored. The functionalization atoms T and T' located at the upper and lower surfaces, respectively, are identical in the case of homogeneous functionalization, while they differ in the case of heterogeneous functionalization. Upon T and T' exchange, an additional reverse heterogeneous configuration is generated. The heterogeneous functionalization of Sc_2CT_2 induces an extraordinary in-plane and out-of-plane piezoelectric effect owing to symmetry breaking. Interestingly, both heterogeneous and its reverse configuration show approximately identical geometrical, energetic, and even elastic properties, but rather different piezoelectric coefficients. The obtained piezoelectric effect is more than ten times larger than the experimentally measured piezoelectricity of MoS_2 -monolayer. Our study suggests a way toward more efficient nanoscale piezoelectric devices based on Sc_2C MXenes.

I. INTRODUCTION

MXenes are a class of 2D transition metal carbides and/or nitrides¹ that have gained considerable attention in recent years. MXene is produced by selectively removing certain layers from the $\text{M}_{n+1}\text{AX}_n\text{T}_x$, known as MAX structure phase, (where $n = 1, 2, \text{ or } 3$; M is a transition metal like Sc, Ti, Cr; A is primarily made up of elements from group IIIA or IVA like Al; X is C or N; and T is the surface termination including O, OH, and/or F atoms) to create a single-layered material. MXenes provide distinct physical and chemical characteristics including exceptional conductivity, high surface area, strong mechanical stability, and top-notch electro- and physico-chemical performance.² MXene materials have been studied for various purposes including energy storage, water purification, electromagnetic interference shielding, and biomedical applications. To that end, there have been many literature reviews and research articles published on MXenes in recent years, covering various aspects of their synthesis, characterization, properties, and applications.³⁻⁹

Regardless of surface functionalization, the distinct

composition of MXenes (diverse combination between M and X constituents) could lead to a distinguishable set of derivatives that open the avenue to tune chemical and/or physical properties of the pristine MXenes. For instance, pristine MXenes, M_{n+1}X_n , exhibit a non-piezoelectric behavior due to the existence of an inversion center of symmetry, however, such piezoelectric behavior can be readily induced via ordered double-transition metal and/or chemical doping.¹⁰

Piezoelectricity is the ability of non-centrosymmetric materials to transform a mechanical field into an electric field, or vice versa.¹¹ This property becomes extremely useful in the persistent quest for the fabrication of nanoscale devices and nano-electromechanical systems (NEMS). Indeed, piezoelectric nanomaterials (PNMs) have been employed for the design of many novel nanodevices, such as nanogenerators, nanosensors, nanodiodes, and nanotransistors, among others.¹²⁻¹⁹ Many 2D materials provide a piezoelectric response, however, most of them solely show an in-plane piezoelectric effect, with a very small portion that possesses out-of-plane piezoelectricity. An out-of-plane piezoelectric response

refers to an induced polarization perpendicular to the 2D plane of the material (xy-plane), which implies the accessibility of bottom/top gate technologies in versatile applications.²⁰ An attempt has been performed in order to induce piezoelectricity in pristine graphene (intrinsically non-piezoelectric) via carbon substitution, where a large in- and out-of-plane piezoelectric response has been retrieved.^{21,22}

Recent studies were concerned with piezoelectricity of MXenes. For instance, Khazaei *et al.*¹⁰ considered a group of MAX phases (iMAX) $((M'_{2/3}M''_{1/3})_2AlC)$ with in-plane ordered double transition metals (M' and M''); where $M' = Mo, W, \text{ and } V$, while $M'' = Y, Sc, \text{ and } Zr$ atoms. The authors confirmed that the F or OH-terminated 2D iMXenes (2D derivatives of iMAX) are generally metallic, while the O-terminated $(Mo_{2/3}Y_{1/3})_2C$, $(Mo_{2/3}Sc_{1/3})_2C$, $(W_{2/3}Y_{1/3})_2C$, and $(W_{2/3}Sc_{1/3})_2C$ iMXenes are semiconductors and possess a giant in-plane piezoelectric coefficient; 45×10^{-10} C/m compared to 4.5×10^{-10} C/m and 38×10^{-10} C/m for in-plane²² and out-of-plane²¹ responses from functionalized graphenes, respectively. Interestingly, the iMXene piezoelectric response is 15 times larger than the experimentally measured e_{11} piezoelectric coefficient of free-standing single layer molybdenum disulfide (MoS_2).²³ Furthermore, in 2019 Tan *et al.* theoretically investigated a series of oxygenated MXenes (M_2CO_2 ; $M = Sc, Y, La$) to be used as ultrathin piezoelectric devices (cantilevers and diaphragms). The considered systems show very strong out-of-plane piezoelectricity which is highly eligible for the intended application.²⁴ An exhaustive inspection for a novel ferroelectric MXene phase with a large piezoelectric response and an exceptional auxeticity has recently been realized.²⁵ In this respect, three types of ferroelectric MXenes phases (type-I: Nb_2CS_2 and Ta_2CS_2 , type-II: Sc_2CO_2 and Y_2CO_2 , type-III: Sc_2CS_2 and Y_2CS_2) were theoretically examined, where giant out-of-plane and in-plane piezoelectric responses have been reported; in particular, the response prompted by type-III MXenes.

In the present study, the piezoelectric effect induced in Sc_2CTT' 2D materials by applying homogeneous ($T = T' = O, S, Se, \text{ and } Te$) and heterogeneous ($T \neq T' = O, S, F, \text{ and } Cl$) functionalizations is investigated. In the considered 2D MXenes, the mixed site functionalized with T- or T'-atoms being metal top on the upper surface and carbon bottom at the lower surface of Sc_2C

nanosheet has been examined. This site has been chosen to break down the inversion symmetry center and to prompt piezoelectricity. Here, the effect of surface termination on piezoelectricity will be discussed. The alteration of electronic and geometrical properties of Sc_2C that are manifested by surface functionalization will be examined. The in- and out-of-plane piezoelectric response will be calculated and analyzed. The origin of different contributions to piezoelectricity and the factors that influence each will be extensively discussed. Thereby we extend previous studies^{24,25} towards a wider range of functionalizing atoms as well as heterogeneous functionalizations.

II. COMPUTATIONAL DETAILS

All calculations within the present study are performed using the plane-wave basis projector-augmented wave (PAW)²⁶ method as implemented in the Vienna ab initio Simulation Package (VASP).^{27,28} The DFT exchange–correlation potential was described by the generalized gradient approximation (GGA) via Perdew–Burke–Ernzerhof (PBE) functional.²⁹ An energy cutoff of 500 eV is applied to control the expansion limit of electron wavefunctions in the plane-wave basis set. For geometry optimization, a conjugate gradient scheme without any symmetry restrictions was used for the total energy and Hellmann-Feynman forces convergence, here set to be 10^{-6} eV and 0.005 eV/Å respectively. A unit cell (5 atoms), including the upper and lower surface functionalization, is considered. A larger supercell ($4 \times 4 \times 1$; 80 atoms) was also examined and nearly identical results are found for both elastic and piezoelectric properties. The Brillouin zone (BZ) was sampled at $12 \times 12 \times 1$ gridmesh that corresponds to 19 irreducible k-points in the 1st BZ. To prevent any spurious interaction along the z-direction between the surface and its image, 15 Å of vacuum space was included. An exploratory calculation using 20 Å of vacuum space has been performed, where the difference in the piezoelectric response does not exceed 0.5%.

The non-vanishing coefficients of elastic stiffness and piezoelectric tensors were obtained using density-functional perturbation theory, which has been shown to give a good estimate of the piezoelectric properties for a wide range of materials.³⁰ The computation of piezoelec-

tric constants will be decomposed into the purely electronic contribution that arises from the clamped-ion calculation and the nuclear “internal-strain” contribution that was obtained after a full relaxation of the strained atomic positions. Indeed, these response properties can be generally expressed as a sum of the two contributions: the purely electronic “clamped-ion” and nuclear “internal-strain”. The static piezoelectric constant e_{iv} , can be given, for instance, as:

$$e_{iv} = e_{iv}^{\text{clamp}} + e_{iv}^{\text{nucl}} \quad (1)$$

Here, e_{iv}^{clamp} refers to the calculation of the variation of polarization after applying a mechanical field, and under clamped-ion conditions, while e_{iv}^{nucl} indicates the piezoelectric response after the full relaxation of the relative positions of atoms induced by the mechanical field i.e. “applied strain”, and can be computed by optimizing the atomic positions within the strained cell.^{31,32} Note that, for those hexagonal 2D systems, the piezoelectric strain parameters, d_{11} , are related to the piezoelectric stress tensors as follows: $d_{11} = e_{11}/(C_{11} - C_{12})$.

III. RESULTS AND DISCUSSION

A. Homogeneous Functionalization

Generally, there are three typical configurations for the surface functionalization of the 2D M_2X layer: 1) M-top

The effect of increasing the functionalization atom size is investigated on homogeneous functionalization by putting $T = T' = O, S, Se,$ and Te . The geometrical, elastic, and piezoelectric properties of these structures are given in Table I. Based on the symmetry analysis of these 2D structures, the stiffness tensor, \mathcal{C} , has only two independent components; C_{11} and C_{12} , while the piezoelectric tensor will show e_{11} and e_{31} for in-plane and out-of-plane response, respectively. The numerical values for both elastic and piezoelectric coefficients are given in Table I, where electronic “clamped-ion” and total “relaxed” in parentheses, i.e. including the nuclear

contribution, constants are reported. From a geometrical point of view, as the functionalization atom size increases the lattice constant, a , increases and the distance of T from the MXene surface increases, see the given values for distances d in Table I; the two Te atoms are placed at 0.24 and 0.16 Å from the upper and lower surfaces, compared to 0.21 and 0.11 Å for O-functionalized Sc_2C MXene.

configuration, where the functionalization atom T is located top to the metal atom on both the upper and lower surfaces of the 2D MXene, 2) X-top configuration, here the T-atom is located top to the X atom, and finally 3) Mixed configuration, where the functionalization atom T is M-top on one side and X-top on the other side of the 2D M_2X nanosheet, see panel a, Figure 1. Piezoelectricity is the second derivative of system energy with respect to a mechanical field, and it exists exclusively in non-centrosymmetric materials. Hence, the larger the symmetry breaking, the larger the piezoelectric response becomes. So, the Mixed configuration is expected to be the most promising configuration for the piezoelectric effect. Based on the literature,^{24,25} Sc_2CT_2 ($T = O$ and S) MXenes show a considerable piezoelectric response and can be considered good candidates for such investigation of different functionalization (atom and type). For each T-atom, three different structures are considered; $T = T'$ (homogeneous functionalization), $T \neq T'$ (heterogeneous functionalization), and $T' \neq T$ (reverse-heterogeneous functionalization), note that T and T' refer to the functionalization on the upper and lower surfaces of 2D MXene monolayer, respectively. A graphical representation of our considered M_2XTT' MXenes, with $T = T'$ for homogeneous functionalization and $T \neq T'$ for heterogeneous and inverted-heterogeneous functionalization, is introduced in Figure 1, panel b.

contribution, constants are reported. From a geometrical point of view, as the functionalization atom size increases the lattice constant, a , increases and the distance of T from the MXene surface increases, see the given values for distances d in Table I; the two Te atoms are placed at 0.24 and 0.16 Å from the upper and lower surfaces, compared to 0.21 and 0.11 Å for O-functionalized Sc_2C MXene.

Since the O-atom has the smallest atomic size among VI-group elements, the O atom will be closer to the 2D MXene surface than the Te atom leading to a more rigid structure for O-functionalized MXene (larger elastic con-

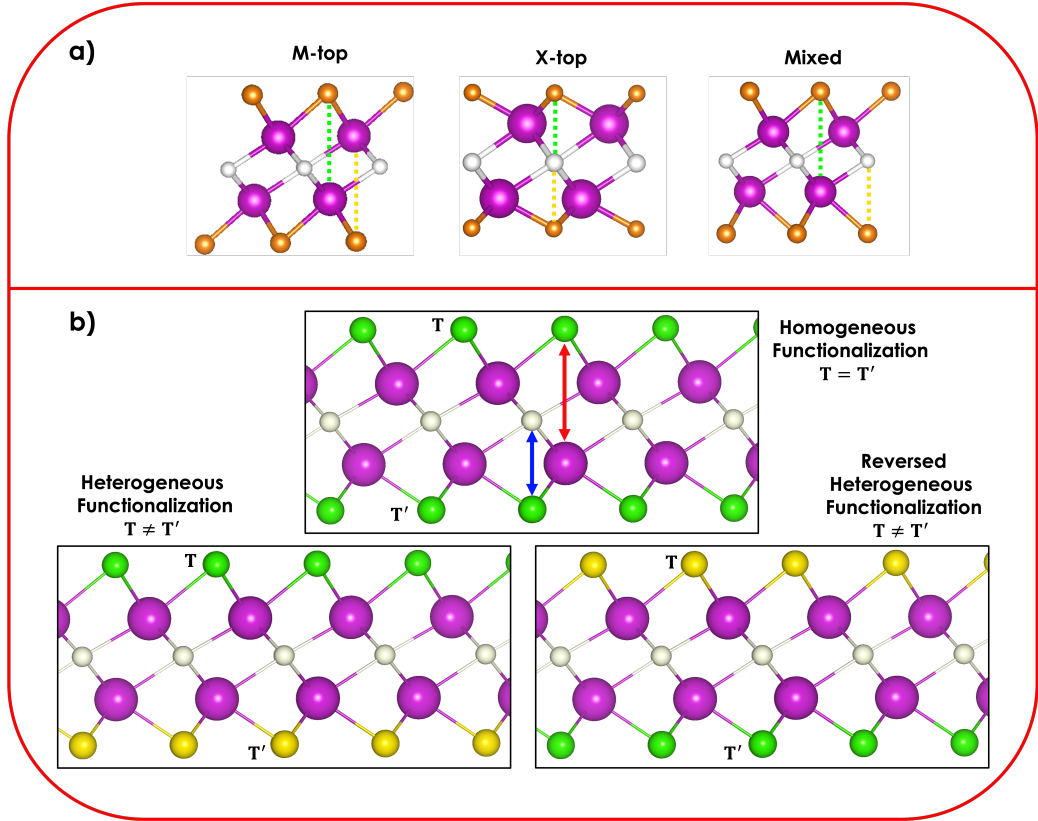


FIG. 1: Graphical representation of the considered Sc₂CTT' MXenes; panel a introduces the three different functionalization configurations: M-top, X-top, and Mixed, while panel b reports various functionalization types: homogeneous ($T = T'$), heterogeneous ($T \neq T'$), and reversed heterogeneous ($T \neq T'$); T and T' are taken as O, S, Se, Te, F, Cl. For the heterogeneous case, one can obtain its reversed configuration by just exchanging between T and T', green and yellow balls. Violet spheres are used to indicate Sc metal, white-grey for carbon, while green and yellow are used to represent functionalization atoms. The red/blue arrow refers to the vertical distances between Sc/C and the upper/lower functionalization atom, respectively.

TABLE I: Geometrical, elastic, and piezoelectric properties of homogeneous functionalized Sc₂CT₂, T = O, S, Se, and Te. Geometrical parameters including lattice constants, a, vertical distance between Sc/C and T-atoms, $d_{M-T}/d_{C-T'}$, respectively, are given in Å. The two independent components of elastic constants, C_{11} and C_{12} , as well as, the in-plane and out-of-plane piezoelectric coefficient, e_{11} and e_{31} , are reported, where the available data within the literature are given for comparison. Both electronic “clamped-ion” and total “relaxed” (values within parentheses) contributions to these response properties (elastic and piezoelectric) are introduced separately.

system	Geometrical parameters			Elastic constant in N/m		Piezoelectric coefficient in pC/m	
	a	d_{M-T}	$d_{C-T'}$	C_{11}	C_{12}	e_{11}	e_{31}
Sc ₂ CO ₂	3.42	0.21	0.11	217 (170)	97 (89)	-440 (277)	112 (213)
Ref. 24				211 (165)	94 (86)	-430 (269)	116 (196)
Ref. 25						(285)	(203)
Sc ₂ CS ₂	3.74	0.23	0.13	154 (94)	64 (65)	-388 (799)	80 (154)
Ref. 25						(867)	(110)
Sc ₂ CSe ₂	3.80	0.23	0.14	140 (88)	56 (58)	-355 (850)	93 (148)
Sc ₂ CTe ₂	3.91	0.24	0.16	125 (78)	49 (55)	-352 (1148)	82 (121)

stant) and a more flexible Te-functionalized one (smaller

elastic constant). This is confirmed by the elastic stiffness constants, C_{11} and C_{12} , in Table I; the total $C_{11} = 170$ and $78 \text{ N}\cdot\text{m}^{-1}$, and $C_{12} = 89$ and $55 \text{ N}\cdot\text{m}^{-1}$, for O and Te functionalized Sc₂C MXene, respectively. Here, the mechanical response dominated by the electronic contribution, while the vibrational contribution is quite small and, generally, has an opposite sign, see Figure 2. Interestingly, the considered 2D functionalized MXenes are generally softer than the conventional 2D graphene and hexagonal boron nitride, h-BN, where C_{11} is greater than $300 \text{ N}\cdot\text{m}^{-1}$.^{21,22}

The considered 2D MXenes show both in-plane and out-of-plane piezoelectric responses. The in-plane response can be deduced from the numerical values of the piezoelectric coefficient e_{11} , which implies an induced polarization through the x-direction as a result of an applied mechanical field in the same direction. The out-of-plane can be observed from the values of e_{31} ; applied

mechanical field through the x-direction and induced polarization via the z-direction. The electronic contribution to the in-plane piezoelectric coefficient decreases going from O towards Te, being -440 pC/m and -352 pC/m for Sc_2CO_2 and Sc_2CTe_2 , respectively. The total contribution to piezoelectricity (sum of electronic and vibrational contributions) is given within the parentheses in Table I. Here, the vibrational contribution predominates for the in-plane piezoelectric response, contrarily to the mechanical response that was dominated by the electronic contribution, an overview of the relative electronic and vibrational contributions is provided in Figure 2. It is worth mentioning that, all considered functionalized MXene have a mixed configuration, and hence the deformation of the cell should lead eventually to a huge change in the polarization, due to the displacement of the T atom. Generally, in the linear regime piezoelec-

tricity describes the polarization induced by an applied mechanical field. Such induced in-plane polarization will increase as the size of the T-atom increases, Table I. This is attributed to the enormous vibrational contribution to the e_{11} due to the more flexible structure in the case of Sc_2CTe_2 , 1500 pC/m, for instance, see Figure 2. The situation is quite different for the out-of-plane piezoelectricity. As the cell is deformed (always in-plane deformation), the T-atom approaches the Sc and C planes of the Sc_2C sheet, and hence the induced out-of-plane polarization decreases as the T-atom size increases. This is apparent from numerical data for the e_{31} constant, starting from 213 pC/m for Sc_2CO_2 till it reaches 121 pC/m for Sc_2CTe_2 . Our obtained results for both mechanical and piezoelectric properties are comparable to the previously reported PW-calculations.^{24,25}

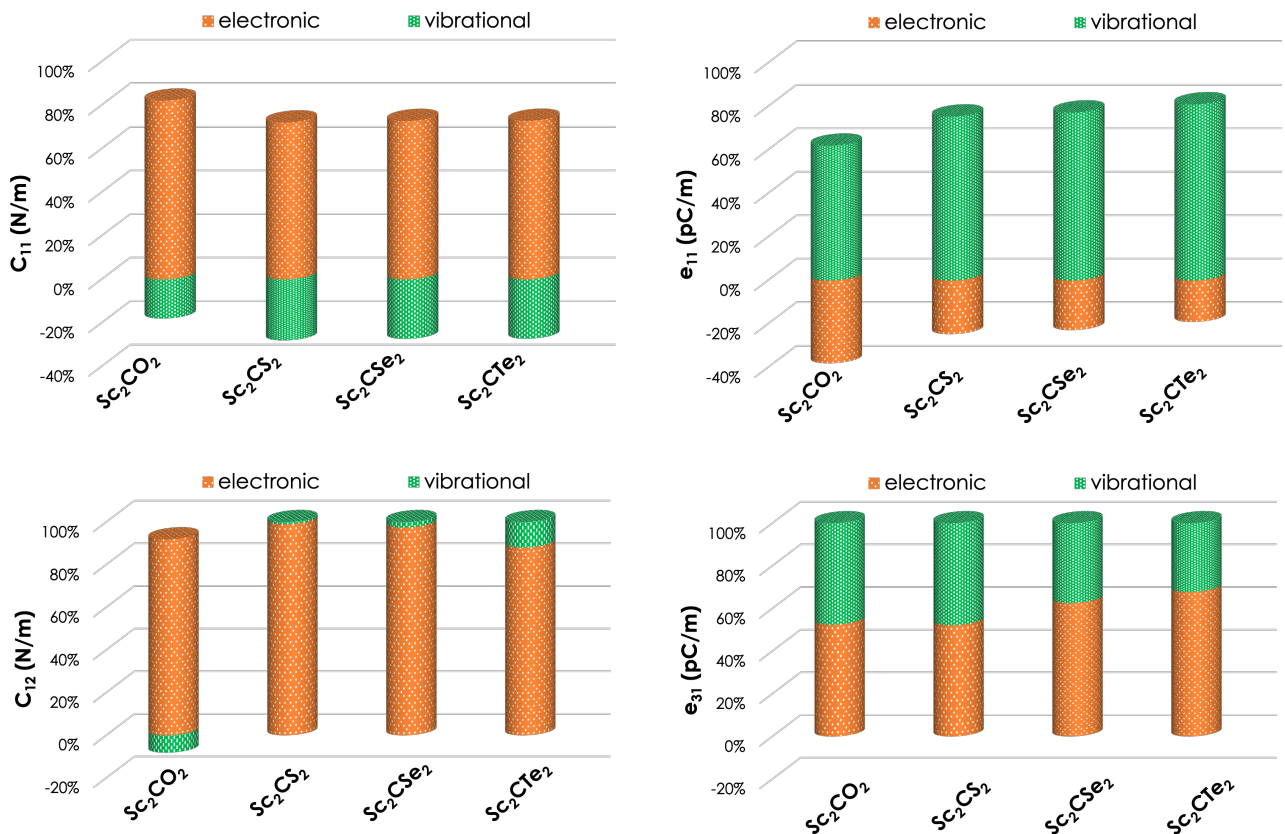


FIG. 2: Electronic (orange) and vibrational (green) contributions to both elastic (left): C_{11} (top) and C_{12} (bottom), and piezoelectric (right): e_{11} (top) and e_{31} (bottom) properties for various Sc_2C MXenes.

The projected density of states (PDOS) for the considered homogeneous functionalization is represented in Figure 3, where the d states of Sc metal, as well as, the p states of carbon and functionalization atoms on the upper and lower surface T and T' (here $T = T'$), are given in panels a, b, c, and d for Sc_2CO_2 , Sc_2CS_2 , Sc_2CSe_2 , and Sc_2CTe_2 , respectively. Sc_2CO_2 , Sc_2CS_2 , and Sc_2CSe_2 systems are being semiconductors with small band gap values of 2.15, 2.07, and 1.77 eV, respectively. While Sc_2CTe_2 MXene shows a conducting behavior with a very small PBE-band gap of 0.48 eV. The conduction bands are dominated by the d states of Sc-metal in all MXene cases, except for Sc_2CTe_2 structure. On the other hand, the valence band is independent on the size of the functionalization atom. The main contributions to the valence bands are the d and p states of Sc and C atoms, respectively, for smaller functionalization atoms with domination of other orbitals as the size of the functionalization atoms increase, Figure 3. Apparently, the contribution of p states of T and T' atoms in the valence band, is increasing from O to Te, which is correlated to their polarizability trend. This leads eventually to the appearance of particular DOS for Sc_2CTe_2 structure; panel d in Figure 3. Although different levels of calculation are considered, our obtained PBE-band gap for Sc_2CO_2 is comparable to previously reported HSE06-band gap of 2.86 eV²⁴ or 2.90 eV.²⁵

B. Heterogeneous Functionalization

Here, the most common elements used for the functionalization of MXenes (O, S, F, and Cl) were considered in order to investigate the influence of such heterogeneous functionalization on both geometrical and piezoelectric properties of Sc_2CT MXene. In the heterogeneous functionalization, the T-atom on the upper surface differs from the functionalization atom on the lower surface, T', see Figure 1, panel b. Since, we consider exclusively the mixed configuration of the MXene, the functionalization on the upper surface is metal top (M-top), while that on the lower surface is carbon bottom (C-bottom). The exchange between T and T' has been investigated as well, where the most stable structure is indicated. Indeed, the

relative stability between the two considered heterogeneous functionalization (T-atom on the upper surface in one case, and its reverse configuration with yellow-atoms being at the bottom surface, Figure 1) is found to be insignificant. However, the particular preference of some functionalization atoms to be M-top or C-bottom can be deduced from the given data in Table II. For instance, the oxygen prefers to be M-top if it exists with sulfur, however, when it comes with halogen (F or Cl), the configuration with halogen atom at M-top is 0.37 and 0.07 eV more stable for F and Cl atoms, respectively. The big size of the Cl-atom, compared to F-atom, plays a crucial role in such stability, see geometrical parameters in Table II. The sulfur atom is less electronegative than the oxygen, and hence the halogen (being F or Cl) prefers the M-top site, with an energy difference of 0.23 eV and 0.27 eV for F and Cl functionalized MXenes, respectively.

TABLE II: Geometrical (lattice constant, a, and distances, $d_{\text{M-T}}$ and $d_{\text{C-T}'}$) and Energetic (total energy, E, and energy difference, ΔE) parameters of heterogeneous functionalized Sc_2C . The order is that the first atom is M-top and the second one is C-bottom.

Functionalization elements	a	$d_{\text{M-T}}$	$d_{\text{C-T}'}$	E	ΔE
O,S	3.59	0.18	0.13	-37.95299	0
S,O	3.52	0.25	0.11	-37.55257	-0.40
O,F	3.29	0.23	0.16	-38.17004	0
F,O	3.29	0.25	0.15	-38.54052	0.37
O,Cl	3.39	0.21	0.19	-36.24438	0
Cl,O	3.37	0.28	0.15	-36.31295	0.07
S,F	3.21	0.30	0.17	-34.85030	0
F,S	3.43	0.24	0.18	-35.08130	0.23
S,Cl	3.31	0.29	0.20	-32.83299	0
Cl,S	3.52	0.27	0.18	-33.10317	0.27
F,Cl	3.32	0.24	0.28	-35.24739	0
Cl,F	3.32	0.28	0.16	-35.24947	0.00

The projected density of states (PDOS) for such heterogeneous functionalized Sc_2C MXenes is given in Figure 4, where the red lines represent the d states of Sc-metal, green lines for p states of carbon, while blue and magenta lines are used to indicate, respectively, the p states of functionalization atom, T and T'; here $T \neq T'$. For reverse heterogeneous functionalization (right column within Figure 4), and in order to reduce the ambiguity with respect to heterogeneous, the same color

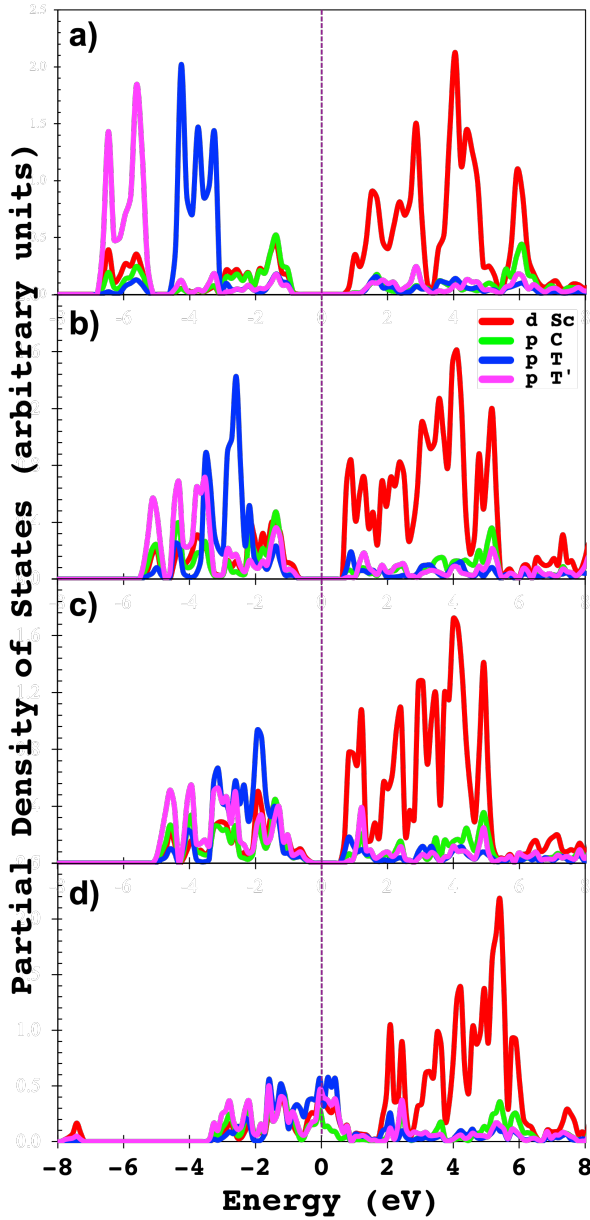


FIG. 3: Projected Density of States (PDOS) for the homogeneous functionalization of Sc_2CT MXene. The d states of Sc metal, as well as, the p states of carbon and functionalization atoms on the upper and lower surface T and T' (here $T = T'$), are given in panels a, b, c, and d for Sc_2CO_2 , Sc_2CS_2 , Sc_2CSe_2 , and Sc_2CTe_2 , respectively. The vertical dashed purple line represents the zero-shifted Fermi level.

Since the energy difference between the heterogeneous and reverse heterogeneous is insignificant, less than 0.5 eV, it will be interesting to see whether the mechanical

is used to represent the same atom whether it is metal top (upper surface) or carbon bottom (lower surface). Similar to homogeneous functionalization, the conduction bands are composed essentially of the d states of Sc-metal, while the valence bands are formed by carbon in most cases, or its bottom-lying functionalization atom, T', Figure 4. Interestingly, Sc_2CFCl and Sc_2CClF systems gave very similar contributions to the DOS, in particular for the valence region confirming the electronic configuration similarity, as confirmed by the zero energy difference obtained in Table II.

and piezoelectric properties differ. The numerical values for the elastic constant, C_{UV} , and the direct piezoelectric coefficients, e_{iV} , are given in Table III. Interest-

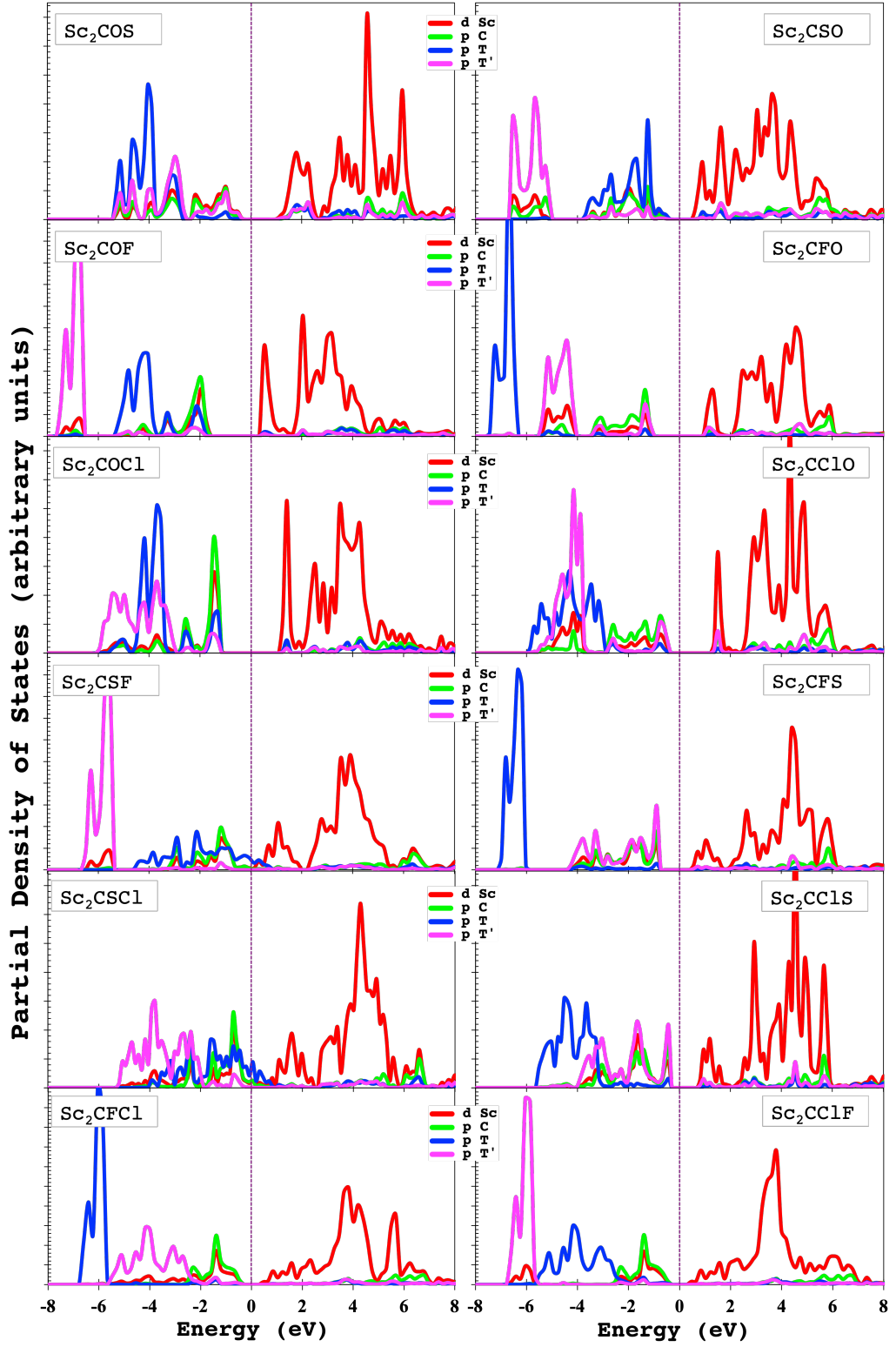


FIG. 4: Projected Density of States (PDOS) for the heterogeneous functionalization of the considered Sc_2C MXene. The d states of Sc metal, as well as, the p states of carbon, T and T' (here $T \neq T'$), are represented by red, green, blue, and magenta lines, respectively. Each heterogeneous functionalization (left column) and its inverse configuration (right column) is reported for comparison. The vertical dashed purple line represents the zero-shifted Fermi level.

ingly, the elastic stiffness constants for the heterogeneous oxygen functionalized Sc_2C MXene decrease when com-

pared to the homogeneous case. For instance, for all O-functionalized systems, the C_{11} never reaches the 170 N.m^{-1} of the homogeneous case, Table I. This is due to the incorporation of the other functionalization atom. Generally, the decrease in the elastic constant makes the system less rigid resulting in easy deformation, and hence some soft modes may exist. Like homogeneous functionalization, the elastic response is predominated by the electronic contribution, the vibrational contribution to the elastic constants is very small and bears an opposite sign with respect to the electronic one. The vibrational contribution to C_{11} and C_{12} equals -54 N.m^{-1} and -1 N.m^{-1} for Sc_2COS ; and -46 N.m^{-1} and -9 N.m^{-1} for Sc_2CSO . For all other functionalized heterogeneous systems, the vibrational contribution to elastic constants have the same (or even less for some systems, Table III) order of magnitude as the OS-functionalized Sc_2C MXene. From the inspection of data within Table III, one can deduce that the mechanical properties for the heterogeneous functionalized Sc_2C systems are not much influenced by the position of T and T'. The difference between the heterogeneous and its reverse configuration is very small, the maximum difference equals 21 N.m^{-1} and 29 N.m^{-1} for the total values of C_{11} and C_{12} of Sc_2CSF and its reverse Sc_2CFS , respectively.

The piezoelectric properties for the six considered heterogeneous functionalized Sc_2C MXene are introduced in Table III, where the electronic and total (values in parentheses) contributions to both the in-plane and out-of-plane direct piezoelectric constants, e_{11} and e_{31} , are reported. Apparently, the piezoelectric responses are extremely sensitive to the alignment of the functionalization atom on the surface, contrarily to the mechanical properties, which are alignment independent. Consequently, the induced polarization will differ when O-atom, for example, being metal-top or carbon-bottom. Hence, in some cases, the two configurations (heterogeneous and its reverse) present completely different responses. For instance, the O,F and F,O configurations introduce completely different numbers for the total and electronic contributions to the in-plane piezoelectric constants; 1086 pC/m and 3093 pC/m for the total contribution, and -10 pC/m and -1486 pC/m for electronic contribution, respectively. Furthermore, the S,F and F,S functionalized Sc_2C have opposite sign for the total values of e_{11} , -160 pC/m and 332 pC/m . Actually, the vibrational contribution to the piezoelectric coefficients

plays a pivotal role for this behavior, being very large and bearing an opposite sign with respect to the electronic. Moreover, such vibrational contribution predominates in the piezoelectric response, since the movement of the functionalization atoms (on the upper and lower surfaces) will lead to a considerable change of the induced polarization.

TABLE III: Elastic and piezoelectric properties of heterogeneous functionalized Sc_2C , and its reverse configuration. The two independent components of elastic constants, C_{11} and C_{12} , as well as, the in-plane and out-of-plane piezoelectric coefficient, e_{11} and e_{31} , are reported, where both electronic ‘‘clamped-ion’’ and total ‘‘relaxed’’ (values within parentheses) contributions are individually reported.

Functionalization elements	Elastic in N/m		Piezoelectric in pC/m	
	C_{11}	C_{12}	e_{11}	e_{31}
O,S	187 (133)	84 (83)	-417 (537)	97 (220)
S,O	183 (137)	72 (63)	-377 (442)	297(336)
O,F	199 (146)	88 (69)	-10 (1086)	295 (416)
F,O	207 (165)	83 (68)	-1486 (3093)	249 (284)
O,Cl	195 (147)	82 (63)	-234 (621)	144 (280)
Cl,O	199 (164)	74 (65)	-204 (107)	119 (184)
S,F	173 (155)	80 (67)	-225 (-160)	332 (358)
F,S	170 (134)	60 (38)	-71 (332)	389 (412)
S,Cl	161 (132)	68 (46)	-169 (78)	215 (218)
Cl,S	159 (123)	55 (37)	-138 (274)	264 (277)
F,Cl	194 (173)	57 (43)	-60 (154)	119 (160)
Cl,F	193 (172)	56 (42)	-60 (151)	119 (159)
H,F (chair) graphene ³³				(-31)
H,F (chair) h-BN ³⁴	(187)	(26)	(181)	(77)
F,H (chair) h-BN ³⁴	(200)	(32)	(84)	(-7)

For out-of-plane piezoelectricity, the values of e_{31} vary considerably from one configuration to another and from functionalization element to another but with, however, a more regular conduct compared to the in-plane response. The total values for the e_{31} coefficient (values within parentheses) are all of the same order of magnitude. The electronic contribution for O,S and S,O functionalized systems introduces two distinct numbers of 97 and 297 pC/m and this can be attributed to the large stability difference (comparing to all other considered functionalization) between the two configurations; O,S configuration is more stable than S,O by 0.40 eV, see Table II. Interestingly, the two F,Cl and Cl,F configurations, which exhibit similar energetic and geometrical parameters except for some vertical distances that depend on F and Cl atomic size (Table II), give almost identical mechanical and piezoelectric responses. This confirms the equal

preference of F and Cl atoms to occupy either M-top or C-bottom sites.

It is worth comparing our obtained results with the available mechanical and piezoelectric properties of heterogeneous surface functionalization of both graphene and h-BN 2D systems. For the graphene system, the two functionalization atoms H and F are C-top, with an atom located over the two irreducible carbons of graphene, leading to a chair-like structure. Since graphene carbons are identical, so the heterogeneous functionalization and its reverse will lead to the same configuration. For h-BN, it would be different if H or F atoms were B- or N-top, as shown in Table III. The lowest obtained e_{31} for Cl,F functionalized Sc_2C -MXene is more than two times larger than the highest obtained value of 77 pC/m for H,F (chair) h-BN.³⁴ Moreover, our largest value of 416 pC/m for e_{31} of the O,F system is interestingly five times larger than that of H,F (chair) h-BN.

To conclude, let us compare the absolute value of piezoelectricity of the best systems we have been discussing in the present study (F,O and its inverse), with that of other 2D and 3D piezoelectric systems. For instance, in-plane piezoelectricity of F,O functionalized Sc_2C -MXene or even its inverse O,F are about 10 and 4 times larger than the in-plane experimentally measured one of the h-MoS₂ monolayers.²³ Furthermore, present converse piezoelectric constants $d_{11} = 25$ pm/V and 10 pm/V for F,O and its inverse are comparable to those of bulk materials like quartz ($d_{11} = 2.3$ pm/V),³⁵ $\text{Si}_{0.83}\text{Ge}_{0.16}\text{O}_2$ ($d_{11} = 5.5$ pm/V),³⁶ GaN ($d_{33} = 3.7$ pm/V),³⁷ AlN ($d_{33} = 5.6$ pm/V).³⁷

IV. CONCLUSION

The present study reports the results of *ab initio* quantum chemical investigations for both homogeneous and heterogeneous functionalized 2D Sc_2C MXenes as potential piezoelectric materials. Here, the mixed configuration of functionalized MXene is exclusively considered, where $T = T'$ for homogeneous functionalization and $T \neq T'$ for heterogeneous functionalization includ-

ing its reverse counterpart. As going down in the periodic table (from O towards Te), the selected MXene becomes less rigid, since the functionalization atom prefers to be located far from the surface. This leads to the presence of some soft vibrational modes and commands a large vibrational contribution to the piezoelectric response. Furthermore, the band gap decreases going from O to Te functionalization and the systems show a conducting behavior, in good accordance with the previously reported studies in the literature. Hence, heterogeneous functionalization and its reverse configuration of MXene have been shown to produce giant both in-plane and out-of-plane piezoelectric responses. Interestingly, both heterogeneous and its reverse functionalization display very similar geometrical, energetic, and even elastic properties, with however extremely distinct piezoelectric properties, which are dominated by vibrational contribution. This is attributed to increasing the induced polarization, when the Sc_2C surfaces functionalized differently. Overcoming the experimental challenge to realize different functionalization at MXene surfaces, the proposed strategy may use these MXenes for improved nanoscale piezoelectric applications.

Acknowledgments

This paper is dedicated to the soul of the late Dr. Ahmed El-Nahas, without whom this project would never have been possible. We hope that we would have made him proud. This contribution was supported by Qatar University High Impact Project QUHI-CAS-21/22-1. The funding by the Deutsche Forschungsgemeinschaft - SFB 1477 "Light-Matter Interactions at Interfaces", project number 441234705" is highly acknowledged.

Access to the High Performance Computing resources provided by the EXPLOR center hosted by the University de Lorraine, is warmly acknowledged. High Performance Computing resources were partially provided by BA-HPC supercomputing facilities sponsored by Bibliotheca Alexandria .

* Electronic address: mshibl@qu.edu.qa

¹ YURY GOGOTSI AND BABAK ANASORI. **The Rise of MXenes.** *ACS Nano*, **13**(8):8491–8494, 2019. Available from:

- <https://doi.org/10.1021/acsnano.9b06394>.
- ² MICHAEL NAGUIB, VADYM N. MOCHALIN, MICHEL W. BARSOUM, AND YURY GOGOTSI. **25th Anniversary Article: MXenes: A New Family of Two-Dimensional Materials.** *Advanced Materials*, **26**(7):992–1005, 2014. Available from: <https://onlinelibrary.wiley.com/doi/abs/10.1002/adma.201304138>.
 - ³ ISMAIL A. M. IBRAHIM, SAFWAT ABDEL-AZEIM, AHMED M. EL-NAHAS, OLIVER KÜHN, CHAN-YEUP CHUNG, AHMED EL-ZATAHRY, AND MOHAMED F. SHIBL. **In Silico Band-Gap Engineering of Cr₂C MXenes as Efficient Photocatalysts for Water-Splitting Reactions.** *The Journal of Physical Chemistry C*, **126**(35):14886–14896, 2022. Available from: <https://doi.org/10.1021/acs.jpcc.2c03622>.
 - ⁴ B. ANASORI, M.R. LUKATSKAYA, AND Y. GOGOTSI. **2D metal carbides and nitrides (MXenes) for energy storage.** *Nature Reviews Materials*, **2**(2):1–17, 2017. Available from: <https://www.nature.com/articles/natrevmats201698#article-info>.
 - ⁵ HYNHO KIM, ZHENWEI WANG, AND HUSAM N. ALSHAREEF. **MXetronics: Electronic and photonic applications of MXenes.** *Nano Energy*, **60**:179–197, 2019. Available from: <https://www.sciencedirect.com/science/article/pii/S2211285519302083>.
 - ⁶ QIU JIANG, CHANGSHENG WU, ZHENGJUN WANG, AURELIA CHI WANG, JR-HAU HE, ZHONG LIN WANG, AND HUSAM N. ALSHAREEF. **MXene electrochemical microsupercapacitor integrated with triboelectric nanogenerator as a wearable self-charging power unit.** *Nano Energy*, **45**:266–272, 2018. Available from: <https://www.sciencedirect.com/science/article/pii/S2211285518300053>.
 - ⁷ LOUISIANE VERGER, VARUN NATU, MICHAEL CAREY, AND MICHEL W. BARSOUM. **MXenes: An Introduction of Their Synthesis, Select Properties, and Applications.** *Trends in Chemistry*, **1**(7):656–669, 2019. Available from: <https://www.sciencedirect.com/science/article/pii/S2589597419300978>.
 - ⁸ RODRIGO MANTOVANI RONCHI, JEVERSON TEODORO ARANTES, AND SYDNEY FERREIRA SANTOS. **Synthesis, structure, properties and applications of MXenes: Current status and perspectives.** *Ceramics International*, **45**(15):18167–18188, 2019. Available from: <https://www.sciencedirect.com/science/article/pii/S0272884219316153>.
 - ⁹ ADIBAH ZAMHURI, GIM PAO LIM, NYUK LING MA, KIAN SEK TEE, AND CHIN FHONG SOON. **MXene in the lens of biomedical engineering: synthesis, applications and future outlook.** *Biomedical engineering online*, **20**(1):1–24, 2021. Available from: <https://biomedical-engineering-online.biomedcentral.com/articles/10.1186/s12938-021-00873-9>.
 - ¹⁰ MOHAMMAD KHAZAEI, VEI WANG, CEM SEVIK, AHMAD RANJBAR, MASAO ARAI, AND SELJI YUNOKI. **Electronic structures of iMAX phases and their two-dimensional derivatives: A family of piezoelectric materials.** *Phys. Rev. Materials*, **2**:074002, Jul 2018. Available from: <https://link.aps.org/doi/10.1103/PhysRevMaterials.2.074002>.
 - ¹¹ JIASHI YANG. *An introduction to the theory of piezoelectricity*, **9**. Springer US, 2005. Available from: <https://www.springer.com/gp/book/9780387235738>.
 - ¹² XUDONG WANG, JINHUI SONG, JIN LIU, AND ZHONG LIN WANG. **Direct-Current Nanogenerator Driven by Ultrasonic Waves.** *Science*, **316**(5821):102–105, 2007. Available from: <https://science.sciencemag.org/content/316/5821/102>.
 - ¹³ YONG QIN, XUDONG WANG, AND ZHONG LIN WANG. **Microfibre–nanowire hybrid structure for energy scavenging.** *Nature*, **451**(7180):809–813, Feb 2008. Available from: <https://doi.org/10.1038/nature06601>.
 - ¹⁴ JUN ZHOU, PENG FEI, YUDONG GU, WENJIE MAI, YIFAN GAO, RUSEN YANG, GANG BAO, AND ZHONG LIN WANG. **Piezoelectric-Potential-Controlled Polarity-Reversible Schottky Diodes and Switches of ZnO Wires.** *Nano Letters*, **8**(11):3973–3977, 2008. PMID: 18823148. Available from: <https://doi.org/10.1021/nl802497e>.
 - ¹⁵ XIAO-MEI ZHANG, MING-YEN LU, YUE ZHANG, LIH-J. CHEN, AND ZHONG LIN WANG. **Fabrication of a High-Brightness Blue-Light-Emitting Diode Using a ZnO-Nanowire Array Grown on p-GaN Thin Film.** *Advanced Materials*, **21**(27):2767–2770, 2009. Available from: <https://onlinelibrary.wiley.com/doi/abs/10.1002/adma.200802686>.
 - ¹⁶ JUN ZHOU, YUDONG GU, PENG FEI, WENJIE MAI, YIFAN GAO, RUSEN YANG, GANG BAO, AND ZHONG LIN WANG. **Flexible Piezotronic Strain Sensor.** *Nano Letters*, **8**(9):3035–3040, 2008. PMID: 18707178. Available from: <https://doi.org/10.1021/nl802367t>.
 - ¹⁷ XUDONG WANG, CHRISTOPHER J. SUMMERS, AND ZHONG LIN WANG. **Large-Scale Hexagonal-Patterned Growth of Aligned ZnO Nanorods for Nano-optoelectronics and Nanosensor Arrays.** *Nano Letters*, **4**(3):423–426, Mar 2004. Available from: <https://doi.org/10.1021/nl035102c>.
 - ¹⁸ CAOFENG PAN, RUOMENG YU, SIMIAO NIU, GUANG ZHU, AND ZHONG LIN WANG. **Piezotronic Effect on the Sensitivity and Signal Level of Schottky Contacted Proactive Micro/Nanowire Nanosensors.** *ACS Nano*, **7**(2):1803–1810, Feb 2013. Available

- from: <https://doi.org/10.1021/nn306007p>.
- 19 RUOMENG YU, CAOFENG PAN, JUN CHEN, GUANG ZHU, AND ZHONG LIN WANG. **Enhanced Performance of a ZnO Nanowire-Based Self-Powered Glucose Sensor by Piezotronic Effect.** *Advanced Functional Materials*, **23**(47):5868–5874, 2013. Available from: <https://onlinelibrary.wiley.com/doi/abs/10.1002/adfm.201300593>.
 - 20 HUICONG LIU, JUNWEN ZHONG, CHENGKUO LEE, SEUNG-WUK LEE, AND LIWEI LIN. **A comprehensive review on piezoelectric energy harvesting technology: Materials, mechanisms, and applications.** *Applied Physics Reviews*, **5**(4):041306, Dec 2018. Available from: <https://doi.org/10.1063/1.5074184>.
 - 21 KHALED E. EL-KELANY, PHILIPPE CARBONNIÈRE, ALESSANDRO ERBA, JEAN-MARC SOTIROPOULOS, AND MICHEL RÉRAT. **Piezoelectricity of Functionalized Graphene: A Quantum-Mechanical Rationalization.** *The Journal of Physical Chemistry C*, **120**(14):7795–7803, Apr 2016. Available from: <https://doi.org/10.1021/acs.jpcc.5b11929>.
 - 22 KH. E. EL-KELANY, PH. CARBONNIÈRE, A. ERBA, AND M. RÉRAT. **Inducing a Finite In-Plane Piezoelectricity in Graphene with Low Concentration of Inversion Symmetry-Breaking Defects.** *The Journal of Physical Chemistry C*, **119**(16):8966–8973, Apr 2015. Available from: <https://doi.org/10.1021/acs.jpcc.5b01471>.
 - 23 HANYU ZHU, YUAN WANG, JUN XIAO, MING LIU, SHAOMIN XIONG, ZI JING WONG, ZILIANG YE, YU YE, XIAOBO YIN, AND XIANG ZHANG. **Observation of piezoelectricity in free-standing monolayer MoS₂.** *Nature Nanotechnology*, **10**(2):151–155, Feb 2015. Available from: <https://doi.org/10.1038/nnano.2014.309>.
 - 24 JIE TAN, YUNHUA WANG, ZONGTAN WANG, XIUJIE HE, YULAN LIU, BIAO WANG, MIKHAIL I. KATSNELSON, AND SHENGJUN YUAN. **Large out-of-plane piezoelectricity of oxygen functionalized MXenes for ultrathin piezoelectric cantilevers and diaphragms.** *Nano Energy*, **65**:104058, Nov 2019. Available from: <https://www.sciencedirect.com/science/article/pii/S2211285519307657>.
 - 25 LEI ZHANG, CHENG TANG, CHUNMEI ZHANG, AND AIJUN DU. **First-principles screening of novel ferroelectric MXene phases with a large piezoelectric response and unusual auxeticity.** *Nanoscale*, **12**(41):21291–21298, 2020. Available from: <https://doi.org/10.1039/D0NR06609E>.
 - 26 G. KRESSE AND D. JOUBERT. **From ultrasoft pseudopotentials to the projector augmented-wave method.** *Phys. Rev. B*, **59**:1758–1775, Jan 1999. Available from: <https://link.aps.org/doi/10.1103/PhysRevB.59.1758>.
 - 27 G. KRESSE AND J. HAFNER. **Ab initio molecular dynamics for liquid metals.** *Phys. Rev. B*, **47**:558–561, Jan 1993. Available from: <https://link.aps.org/doi/10.1103/PhysRevB.47.558>.
 - 28 G. KRESSE AND J. FURTHMÜLLER. **Efficient iterative schemes for ab initio total-energy calculations using a plane-wave basis set.** *Phys. Rev. B*, **54**:11169–11186, Oct 1996. Available from: <https://link.aps.org/doi/10.1103/PhysRevB.54.11169>.
 - 29 JOHN P. PERDEW, KIERON BURKE, AND MATTHIAS ERNZERHOF. **Generalized Gradient Approximation Made Simple.** *Phys. Rev. Lett.*, **77**:3865–3868, Oct 1996. Available from: <https://link.aps.org/doi/10.1103/PhysRevLett.77.3865>.
 - 30 MAARTEN DE JONG, WEI CHEN, HENRY GEERLINGS, MARK ASTA, AND KRISTIN ASLAUG PERSSON. **A database to enable discovery and design of piezoelectric materials.** *Scientific Data*, **2**(1):150053, Sep 2015. Available from: <https://doi.org/10.1038/sdata.2015.53>.
 - 31 GOTTHARD SÁGHI-SZABÓ, RONALD E. COHEN, AND HENRY KRAKAUER. **First-Principles Study of Piezoelectricity in PbTiO₃.** *Phys. Rev. Lett.*, **80**:4321–4324, May 1998. Available from: <https://link.aps.org/doi/10.1103/PhysRevLett.80.4321>.
 - 32 ANDREA DAL CORSO, MICHEL POSTERNAK, RAFFAELE RESTA, AND ALFONSO BALDERESCHI. **Ab initio study of piezoelectricity and spontaneous polarization in ZnO.** *Phys. Rev. B*, **50**:10715–10721, Oct 1994. Available from: <https://link.aps.org/doi/10.1103/PhysRevB.50.10715>.
 - 33 MITCHELL T. ONG AND EVAN J. REED. **Engineered Piezoelectricity in Graphene.** *ACS Nano*, **6**(2):1387–1394, 2012. PMID: 22196055. Available from: <https://doi.org/10.1021/nn204198g>.
 - 34 MOHAMMAD NOOR-A-ALAM, HYE JUNG KIM, AND YOUNG-HAN SHIN. **Dipolar polarization and piezoelectricity of a hexagonal boron nitride sheet decorated with hydrogen and fluorine.** *Phys. Chem. Chem. Phys.*, **16**:6575–6582, 2014. Available from: <http://dx.doi.org/10.1039/C3CP53971G>.
 - 35 R. BECHMANN. **Elastic and Piezoelectric Constants of Alpha-Quartz.** *Phys. Rev.*, **110**(5):1060–1061, 1958.
 - 36 KH. E. EL-KELANY, A. ERBA, P. CARBONNIÈRE, AND M. RÉRAT. **Piezoelectric, Elastic, Structural and Dielectric Properties of Si_{1-x}Ge_xO₂ Solid Solution: a Theoretical Study.** *J. Phys.: Cond. Matter*, **26**:205401, 2014.

- ³⁷ I. L. GUY, S. MUENSIT, AND E. M. GOLDYS. **Ex-**
tensional Piezoelectric Coefficients of Gallium Ni-
tride and Aluminum Nitride. *Appl. Phys. Lett.*,
75(26):4133–4135, 1999.